

Control of spatiotemporal patterns in the Gray–Scott model

Y. N. Kyrychko,^{1,a)} K. B. Blyuss,¹ S. J. Hogan,¹ and E. Schöll²

¹*Department of Engineering Mathematics, University of Bristol, Bristol BS8 1TR, United Kingdom*

²*Institut für Theoretische Physik, Technische Universität Berlin, 10623 Berlin, Germany*

(Received 29 April 2009; accepted 10 November 2009; published online 9 December 2009)

This paper studies the effects of a time-delayed feedback control on the appearance and development of spatiotemporal patterns in a reaction-diffusion system. Different types of control schemes are investigated, including single-species, diagonal, and mixed control. This approach helps to unveil different dynamical regimes, which arise from chaotic state or from traveling waves. In the case of spatiotemporal chaos, the control can either stabilize uniform steady states or lead to bistability between a trivial steady state and a propagating traveling wave. Furthermore, when the basic state is a stable traveling pulse, the control is able to advance stationary Turing patterns or yield the above-mentioned bistability regime. In each case, the stability boundary is found in the parameter space of the control strength and the time delay, and numerical simulations suggest that diagonal control fails to control the spatiotemporal chaos. © 2009 American Institute of Physics. [doi:10.1063/1.3270048]

Various real-life systems exhibit complex dynamical regimes, including spatial patterns and spatiotemporal chaos. An important issue is the possibility of attaining a desired state by means of some external influence on the system. Time-delayed feedback uses the difference between current state of the system and its state some time ago to provide an efficient tool to control system's dynamics. In particular, this approach allows one to effectively switch between different spatiotemporal regimes in the system. In this paper, we show how the time-delayed feedback control can be used to control spatiotemporal chaos, as well as to provide a transition from traveling waves to stationary periodic patterns.

I. INTRODUCTION

Spatially extended systems arise in modeling of various physical, biological, chemical, and engineering phenomena, and an ultimate understanding of such systems gives one the ability to control them in order to achieve desired behavior or spatial patterns. Since many systems in nature exhibit intrinsic chaotic behavior, control of chaos in spatially extended systems has recently become an active and important area of research.

Control of a dynamical system in a chaotic state usually requires application of some external perturbation in order to achieve a desired type of behavior, such as a steady state, regular, or quasiperiodic oscillations. A number of different methods and techniques have been suggested in order to control chaos.¹ For systems without spatial extension, standard approaches include the Ott–Grebogi–Yorke scheme² and time-delayed feedback control (TDFC).³ TDFC schemes are straightforward to implement and can also be adapted to control spatially extended systems. These schemes are based on the use of the difference between the system variables at the

current moment of time and their values at some time in the past. For low-dimensional systems, TDFC has been successfully used to stabilize unstable steady states,^{4–6} as well as unstable periodic orbits⁷ in a number of physical and biological systems.¹

More recently, TDFC has been used to control spatiotemporal chaos and pattern formation in chemical reactions. Close to the onset of uniform oscillations, it is possible to reduce any reaction-diffusion system to an amplitude equation, called the complex Ginzburg–Landau equation (CGLE).⁸ The CGLE helps to understand the underlying dynamics of the reaction-diffusion systems close to the bifurcation point, however, it does not provide a lot of information about the dynamics far away from the onset of oscillations. Beta and Mikhailov have shown analytically that global TDFC cannot stabilize uniform oscillations when the system is in the spatiotemporally chaotic regime.^{9,10} At the same time, local time-delay feedback control which also includes spatial feedback terms has been shown to be effective in stabilizing traveling waves in CGLE in one and two spatial dimensions.^{11,12}

In globally coupled reaction-diffusion systems, which arise in modeling semiconductor nanostructures, global or local TDFC and its various modifications have proven successful in stabilizing unstable spatiotemporal oscillations.^{13–15} Unstable rigid rotation of spiral waves has also been stabilized by TDFC.¹⁶ Pulse propagation in the FitzHugh–Nagumo reaction-diffusion model has recently been shown to be controllable by local TDFC or nonlocal instantaneous feedback.¹⁷

From a practical perspective, there are several issues that have to be taken into account when considering implementation of specific TDFC schemes. One such aspect concerns the spatial range over which the control has to be applied. Ahlborn and Parlitz¹⁸ have recently shown how one can use multiple time-delayed control applied at a number of control points to stabilize plane waves in the CGLE, while Bleich

^{a)}Electronic mail: y.kyrychko@bristol.ac.uk.

and Socolar¹⁹ have illustrated stabilization of periodic orbits in chaotic CGLE using local control. Another problem is that most examples of TDFC for spatially extended systems such as, for instance, one-dimensional chaotic CGLE (Ref. 19) and spatiotemporally chaotic semiconductor laser arrays,²⁰ use diagonal control with symmetric gain, which may be quite restrictive. In the case of optical systems such as laser devices it is possible to have a nondiagonal coupling, realized experimentally using an optical phase as an additional control parameter.^{4,6} Hence, it is important to consider the influence of various TDFC schemes on the dynamics of the system and analyze different types of spatiotemporal dynamical regimes that can be achieved.

In this paper we perform a systematic study of the effects of local TDFC on spatiotemporal dynamics in a two-component reaction-diffusion system. As a testbed for this analysis we use the paradigmatic Gray–Scott model derived in the context of chemical reactions. It has already been shown using extensive numerical simulations that the Gray–Scott model supports a wide range of spatiotemporal dynamics, including stationary inhomogeneous patterns, traveling fronts and pulses, as well as spatiotemporal chaos. A particular feature of this system, which makes it different from other reaction-diffusion models, is the occurrence of pulse splitting, where a traveling pulse leaves in its wake other pulses propagating in different directions.

The outline of this paper is as follows. In Sec. II we introduce the Gray–Scott system. Section III contains an analysis of the effects of TDFC on spatiotemporal chaos. In Sec. IV various TDFC schemes are applied to propagating pulses. The paper concludes with a summary of our findings, together with a consideration of their implications.

II. GRAY–SCOTT SYSTEM

In order to analyze the effects of TDFC on the spatiotemporal dynamics in reaction-diffusion systems, we consider the Gray–Scott model, which describes a cubic autocatalytic chemical reaction of the type²¹



where U is continuously supplied into an open flow reactor, and the product P is removed. The first equation represents an autocatalytic process, in which two molecules of species V produce $3V$ through interaction with a molecule of species U . If the system were closed, then by virtue of irreversibility of the two reactions, all reactants would eventually turn into a product and be removed. However, when the reactor is continuously fed with a uniform flow of species U , it is possible to maintain far-from-equilibrium conditions, in which a wide range of possible dynamics can be observed. In experiments, a gel is used as a medium to prevent the occurrence of convective currents.²² The kinetic equations for the system (1) can be written after some rescaling as

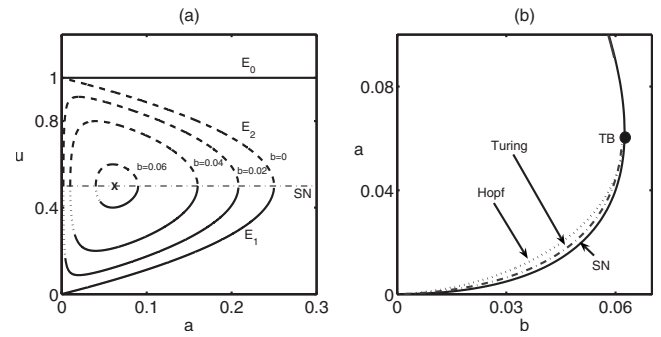


FIG. 1. (a) Bifurcation diagram of the Gray–Scott system (2) without diffusion. Solid lines correspond to stable steady states, dashed to the unstable steady state E_2 , dotted to the Hopf unstable steady state E_1 , and dot-dashed indicates a saddle-node (SN) line. The cross (X) indicates the location of the Takens–Bogdanov point. (b) Phase diagram in (a, b) space. Solid line is the boundary of saddle-node bifurcation, dotted line is the boundary of Hopf bifurcation, and dot-dashed line is Turing instability boundary. TB is the Takens–Bogdanov point.

$$\frac{\partial u}{\partial t} = -uv^2 + a(1-u) + D_u \nabla^2 u = f(u, v) + D_u \nabla^2 u, \quad (2)$$

$$\frac{\partial v}{\partial t} = uv^2 - (a+b)v + D_v \nabla^2 v = g(u, v) + D_v \nabla^2 v,$$

where u and v are the concentrations of the species U and V , respectively, a is the inflow rate, $a+b$ is the removal rate of V from the reaction, and D_u and D_v are the diffusion coefficients of the two species.

The system (2) can possess up to three homogeneous steady states. There is a trivial steady state,

$$E_0 = (u_0, v_0) = (1, 0), \quad (3)$$

which exists for all parameter values and corresponds to a steady flow without reaction. Provided

$$d \equiv 1 - 4(a+b)^2/a > 0, \quad (4)$$

the system has two nontrivial steady states,

$$E_1 = (u_1, v_1) = \left(\frac{1}{2}(1 - \sqrt{d}), \frac{1}{2} \frac{a}{a+b} (1 + \sqrt{d}) \right) \quad (5)$$

and

$$E_2 = (u_2, v_2) = \left(\frac{1}{2}(1 + \sqrt{d}), \frac{1}{2} \frac{a}{a+b} (1 - \sqrt{d}) \right). \quad (6)$$

Linear stability analysis indicates that the trivial steady state E_0 is always linearly stable (even with respect to spatially inhomogeneous perturbations), while the steady state E_2 is unstable with respect to homogeneous perturbations for any parameter values for which it exists. Figure 1 shows a bifurcation diagram for the spatially homogeneous Gray–Scott model, as well as a phase diagram in (a, b) space. One of the features is that when the inflow a is large enough ($a > 1/4$), the production of V is suppressed, and as a result the only fixed point of the system is the trivial steady state E_0 , as shown in Fig. 1(a).

In Fig. 1(b) the saddle-node bifurcation curve is given by

$$a^{SN} = \frac{1}{8}[1 - 8b \pm \sqrt{1 - 16b}]. \tag{7}$$

To the right of a^{SN} only the trivial steady state E_0 exists. As a^{SN} is crossed, two more states E_1 and E_2 appear. While the state E_2 is always unstable, the fixed point E_1 may lose its stability via a Hopf bifurcation. The boundary of this bifurcation is given by²³

$$a^H = \frac{1}{2}[\sqrt{b} - 2b - \sqrt{b(1 - 4\sqrt{b})}]. \tag{8}$$

This boundary starts at $(a,b)=(0,0)$ and follows the lower branch of the saddle-node curve until it coincides with it at a Takens–Bogdanov point $(a,b)=(1/16,1/16)$. The steady state E_1 is stable above the Hopf boundary and unstable below it. It is noteworthy that the stability of the limit cycle that appears due to the Hopf bifurcation varies along the Hopf curve: it is stable for $b < 0.035$ and unstable for $b > 0.035$.

Another way in which a state E_1 may lose its stability is via a Turing bifurcation, which may give rise to stationary inhomogeneous patterns. Linear stability analysis in this case shows that the Turing bifurcation occurs when the ratio of the two diffusion coefficients $\sigma = D_u/D_v$ satisfies the condition²³

$$[\sigma(a + b) - (v_1^2 + a)]^2 > 4\sigma(a + b)(v_1^2 - a), \tag{9}$$

where v_1 is the steady state value of the species V given in Eq. (5). The higher σ , the wider is the region in (a,b) space where Turing bifurcation can be observed. The steady state E_1 is stable with respect to spatially inhomogeneous perturbations above the Turing boundary and unstable below it. For sufficiently high values of σ , the boundary of Turing bifurcation will move above the boundary of Hopf bifurcation. For $\sigma=2$, which will be used in numerical simulations later in this paper, the region of Turing instability is almost entirely contained within the parameter region of Hopf instability, as shown in Fig. 1(b). Interaction of these two instabilities gives rise to spatiotemporal chaos and mixed modes having time-dependent spatial structures.^{23,24} In Fig. 1(b), the region of spatiotemporal chaos is narrow and bounded by the Turing boundary from the top and the saddle-node curve from the bottom. It is noteworthy that very close to the Takens–Bogdanov point one has a Turing instability where stationary inhomogeneous patterns are observed.

It has already been mentioned that the Gray–Scott system exhibits a wide range of dynamical behaviors. In the parameter regime away from Turing and Hopf areas, the system always ends up in either the homogeneous trivial steady state E_0 or state E_1 . The simplest inhomogeneous state is represented by a stationary nonuniform pattern arising from a Turing bifurcation. Besides these temporally stationary structures, the Gray–Scott system is able to support standing or traveling waves and fronts (the latter refer to heteroclinic connections between E_0 and E_1). Traveling waves occur in the parameter region outside the saddle-node boundary. At a higher level of complexity are the mixed modes, describing time-dependent spatial structures, the so-called self-replicating patterns and spatiotemporal chaos.²⁴ The self-

replicating patterns represent heteroclinic connections between the trivial homogeneous state and a spatially periodic pattern.

III. CONTROL OF SPATIOTEMPORAL CHAOS

In this section we concentrate on the parameter regime where the system exhibits spatiotemporal chaos and consider several schemes for the control of this state based on TDFC. This approach has already been used to control spatiotemporal chaos in globally coupled reaction-diffusion systems,^{13,15} as well as in reaction-diffusion systems with global control.^{9,25}

Formally, the locally controlled Gray–Scott model can be written as

$$\begin{aligned} \frac{\partial}{\partial t} \begin{pmatrix} u \\ v \end{pmatrix} &= \begin{pmatrix} f(u,v) \\ g(u,v) \end{pmatrix} + \begin{pmatrix} D_u & 0 \\ 0 & D_v \end{pmatrix} \nabla^2 \begin{pmatrix} u \\ v \end{pmatrix} \\ &+ KA \begin{pmatrix} u(t - \tau) - u(t) \\ v(t - \tau) - v(t) \end{pmatrix}, \end{aligned} \tag{10}$$

where K is the control strength which can be either positive or negative, $\tau > 0$ is the time delay, and A is a 2×2 matrix which describes the particular coupling of the control term. First we consider the case when the control of each variable depends only on the history of that variable. For single-species control, the matrix A takes the form

$$A_u = \begin{pmatrix} 1 & 0 \\ 0 & 0 \end{pmatrix} \quad \text{or} \quad A_v = \begin{pmatrix} 0 & 0 \\ 0 & 1 \end{pmatrix} \tag{11}$$

for control only in u (activator control) and only in v (inhibitor control), respectively.

In the case of activator control, we look for solutions of the system (10) linearized near $E_1=(u_1, v_1)$ in the form

$$\begin{pmatrix} \tilde{u} \\ \tilde{v} \end{pmatrix} = \begin{pmatrix} C_1 \\ C_2 \end{pmatrix} e^{iqx + \lambda t},$$

where $u = u_1 + \tilde{u}$, $v = v_1 + \tilde{v}$, $C_{1,2}$ are constants, q is the wave-number of the perturbation, and λ is the corresponding growth rate. Substituting this into the system (10) with A_u from Eq. (11) yields the following characteristic equation:

$$\begin{vmatrix} -v_1^2 - a - D_u q^2 + K[e^{-\lambda\tau} - 1] - \lambda & -2(a + b) \\ v_1^2 & a + b - D_v q^2 - \lambda \end{vmatrix} = 0. \tag{12}$$

In the absence of control ($K=0$), it follows from this equation that the uniform mode with $q=0$ is the most unstable, i.e., it has an eigenvalue with the largest positive real part. Since the diffusion plays a stabilizing role, all other modes with $q > 0$ will be more stable, as is confirmed by numerical solution of Eq. (12) shown in Fig. 2. For this reason, it suffices to control the uniform mode $q=0$ to achieve complete stabilization of the steady state E_1 for any spatially inhomogeneous perturbation. When $q=0$, Eq. (12) can be written as $\lambda^2 + \lambda[v_1^2 - b - K(e^{-\lambda\tau} - 1)] + (a + b)[v_1^2 - a + K(e^{-\lambda\tau} - 1)] = 0$. (13)

In order to find the control strength K that can stabilize the

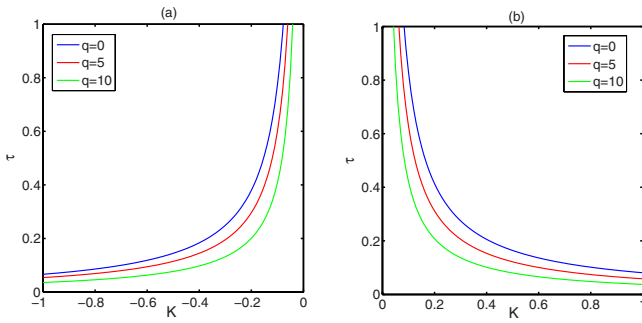


FIG. 2. (Color online) Stability boundaries of the homogeneous steady state E_1 from the characteristic equation (12). In both cases, the steady state E_1 is stable above the boundary for $q=0$ described by Eq. (14). (a) Activator control. (b) Inhibitor control. Parameter values are $a=0.028$, $b=0.053$, $D_u=2 \times 10^{-5}$, and $D_v=10^{-5}$.

steady state E_1 for each value of the time delay τ , we compute the stability boundary in the (K, τ) plane by setting $\lambda=i\omega$ in Eq. (13). Separating real and imaginary parts gives the following system:

$$-\omega^2 + (a+b)(v_1^2 - a - K) - K\omega \sin \omega\tau + (a+b)K \cos \omega\tau = 0,$$

$$\omega(-b + v_1^2 + K) - \omega K \cos \omega\tau - (a+b)K \sin \omega\tau = 0.$$

This system can be solved to yield the pair (K, τ) as parametrized by ω ,

$$K = -\frac{1}{2} \frac{[(a+b)^2 + \omega^2][(a-v_1^2)^2 + \omega^2] - 4\omega^2 b v_1^2}{(a-v_1^2)^2(a+b)^2 + \omega^2(a+v_1^2)}, \tag{14}$$

$$\tau = \frac{1}{\omega} \left[\arctan\left(\frac{2\omega}{K} - \frac{4(a+b)v_1^2\omega}{K[(a+b)^2 + \omega^2]}\right) \pm n\pi \right],$$

$$n = 0, 1, 2, \dots,$$

where \arctan corresponds to the principal value of \arctan . We are only interested in the branch $n=0$, as for other values of n the corresponding control term in the system (10) will be very large compared to other terms, making it unfeasible for practical purposes. In Fig. 2(a) we show this stability boundary, which corresponds to $q=0$, together with stability

boundaries when spatially inhomogeneous perturbations are taken into consideration. For any $q>0$, these boundaries lie below the stability boundary for the uniform mode, as we have explained earlier. Figure 2(b) shows the results of computation of the stability boundary in the (K, τ) plane for inhibitor control. One can note the approximate symmetry between the stability boundaries for activator and inhibitor control up to a reverse of the sign of the control strength. This is due to the fact that the inhibitor control would result in the characteristic equation similar to Eq. (13), but with the term $(a+b)K[e^{-\lambda\tau}-1]$ being replaced by $-(v_1^2+a)K[e^{-\lambda\tau}-1]$, where the difference in the absolute values of $(a+b)$ and (v_1^2+a) is less than 10%. Finally, we note that it is only possible to stabilize the steady state E_1 for negative values of the control strength K in the case of activator control and only for positive K in the case of inhibitor control.

In order to understand the full dynamics of the system (10) with TDFC, we solve this system numerically and record the ultimate stage of time evolution. System parameters are fixed and taken to be $D_u=2 \times 10^{-5}$ and $D_v=10^{-5}$, while kinetic parameters are $a=0.028$ and $b=0.053$. In each case we solve system (10) on an interval of length $L=2.5$ using an explicit Euler scheme with a spatial resolution of 256 mesh points, a time step of $\Delta t=0.05$, and periodic boundary conditions. Initial conditions are chosen to be a random localized perturbation of E_0 in the middle of the domain which then evolves into a spatiotemporally chaotic state. After the spatiotemporal chaos has developed, control is switched on at $t=3000$ and its effects on the time evolution are studied. Time durations of each run are 6000 in the regime of spatiotemporal chaos and 7000 in the case of control of traveling waves.

The results of numerical simulations of activator/inhibitor control are shown in Figs. 3(a) and 3(b). First of all, one can note a characteristic scaling of $|K| \propto 1/\tau$, which is quite natural bearing in mind that if the time delay is small, then the absolute value of the difference $|u(t-\tau)-u(t)|$ (or $|v(t-\tau)-v(t)|$) is small, and therefore a much higher value of the control strength $|K|$ is required to achieve a significant effect on the dynamics. In the case of activator control with $K<0$ or inhibitor control with $K>0$, the only possible transition is from a spatiotemporally chaotic state to a nontrivial

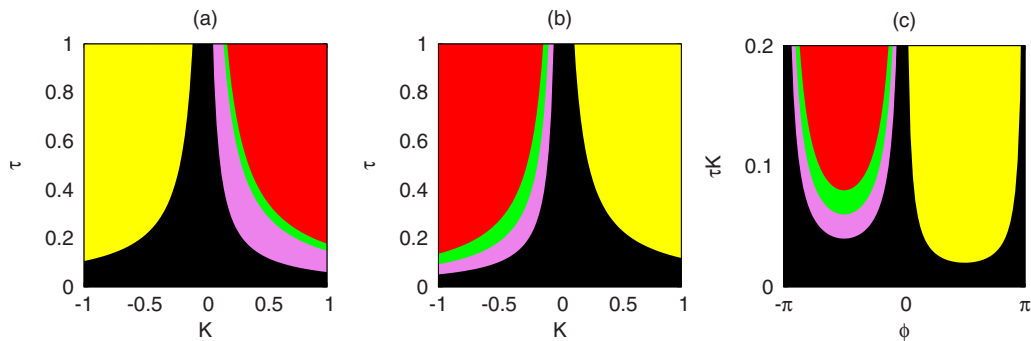


FIG. 3. (Color online) Control domain of spatiotemporal chaos. (a) Activator control. (b) Inhibitor control. (c) Phase diagram for nondiagonal control (15). (a) Specific final states are: the spatiotemporal chaos (black), to the right of it is a stable mixed (Turing-Hopf) state (pink), followed by an area of coarsening (green) and a bistability between traveling waves and a trivial steady state E_0 (red). In the area to the left of the black region the final state is a uniform non-trivial steady state E_1 (yellow). In (b) and (c) the order of regimes from left to right is reversed. Parameter values are $a=0.028$, $b=0.053$, $D_u=2 \times 10^{-5}$, and $D_v=10^{-5}$.

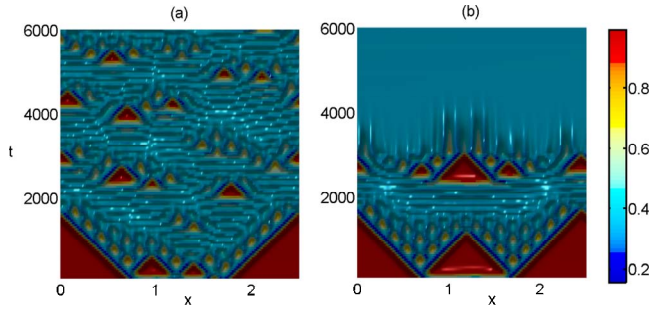


FIG. 4. (Color online) Space-time plot in the case of activator control. (a) Spatiotemporal chaos. (b) Nontrivial steady state E_1 . The color code corresponds to the values of $u(x,t)$. Parameter values are $a=0.028$, $b=0.053$, $D_u=2 \times 10^{-5}$, $D_v=10^{-5}$, (a) $K=-0.4$, $\tau=0.1$ and (b) $K=-0.8$, $\tau=0.6$. Control is switched on at $t=3000$.

homogeneous state E_1 , as shown in Fig. 4. One should note that when the control strength is not sufficiently large, the system remains in the spatiotemporally chaotic state, as shown in Fig. 4(a). The numerical boundary separating spatiotemporally chaotic state from a stable nontrivial homogeneous state shown in Figs. 4(a) and 4(b) coincides with an earlier found analytical expression for this boundary given by Eq. (14).

In the opposite case, for activator control with $K > 0$ or inhibitor control with $K < 0$, when the control strength $|K|$ and the time delay τ are sufficiently small, the system remains in the state of spatiotemporal chaos [see Fig. 5(a)]. For higher values of $|K|\tau$ one observes stable mixed or Turing–Hopf modes shown in Fig. 5(b). These states are characterized by both spatial and temporal periodicities. Earlier work on codimension two Turing–Hopf states suggests that generically these are quite stable close to the Turing–Hopf boundary, and away from it they turn into either pure Hopf oscillations or Turing structures.

In the case of the Gray–Scott system this does not happen as the Turing instability boundary is completely enclosed inside the region of Hopf instability.

For yet higher values of $|K|\tau$, isolated regions coalesce, and the system exhibits coarsening, as shown in Fig. 5(c). Further increase in $|K|\tau$ leads to a bistability between a homogeneous trivial state E_0 or a localized pulse traveling with a constant velocity. This bistability here refers to a regime where for the same values of parameters and random initial conditions, the system will evolve either as shown in Fig. 5(d), i.e., develop into a localized pulse, or it will develop in a manner qualitatively similar to the one shown in Fig. 4(b), except that the evolution leads to a uniform trivial steady state E_0 . We also note that the time-delayed feedback of the form used in Eq. (10) is noninvasive only in the case of stabilization of a uniform steady state E_1 . In all other situations, although the feedback term does not vanish, its norm constitutes less than 10% compared to other terms in the system (10).

Another possibility of control is the so-called diagonal control, which corresponds to the unity coupling matrix A . This type of control has been successfully used to stabilize unstable spatiotemporal breathing in a reaction-diffusion model for the double barrier resonant tunneling diode.¹⁵ Numerical simulations suggest that for the Gray–Scott model this type of control does not qualitatively affect the dynamics as it leaves the system in a spatiotemporally chaotic state for any values of the control strength K and the time delay τ .

In the case of nondiagonal control that involves both species we introduce a variable phase ϕ into the coupling matrix as follows:

$$A = \begin{pmatrix} \cos \phi & \sin \phi \\ -\sin \phi & \cos \phi \end{pmatrix}. \tag{15}$$

Such kind of control occurs, for example, in laser systems, where the optical phase can be used as an additional control parameter.^{6,29} Figure 3(c) shows that for this type of control, the final state of the system is completely determined by the sign and size of nondiagonal control terms and shows no dependence on the values of the diagonal coupling terms. It is worth noting that in the case of *negative feedback* ($-\pi \leq \phi \leq 0$), i.e., when the roles of activator and inhibitor in the control term are reversed, one observes a range of possible dynamical regimes, such as stable Turing–Hopf modes, coarsening and bistability between traveling waves and a trivial steady state E_0 . On the other hand, for *positive feedback* with $0 \leq \phi \leq \pi$, the only possible transition is from a spatiotemporally chaotic state to a uniform nontrivial steady state E_1 .

Beta and Mikhailov have previously shown for the CGLE that in the Benjamin–Feir regime, which gives rise to spatiotemporal chaos, the global TDFC is unable to stabilize uniform oscillations.⁹ Our simulations suggest that a similar conclusion holds for local time-delayed feedback: while it is possible to recover homogeneous states, as well as stable mixed modes, it appears impossible to stabilize uniform oscillations in a reaction-diffusion system.

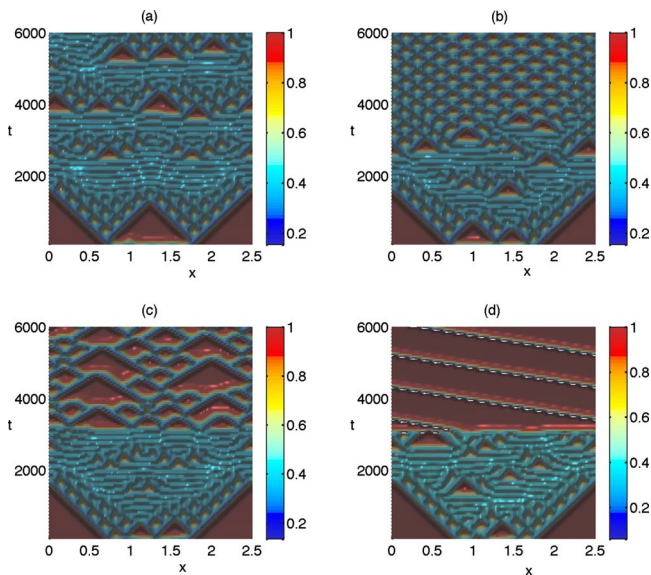


FIG. 5. (Color online) Space-time plot in the case of inhibitor control. (a) Spatiotemporal chaos. (b) Mixed (Turing–Hopf) mode. (c) Coarsening. (d) Transition to traveling waves. Parameter values are $a=0.028$, $b=0.053$, $D_u=2 \times 10^{-5}$, $D_v=10^{-5}$, (a) $K=-0.05$, $\tau=0.3$, (b) $K=-0.3$, $\tau=0.35$, (c) $K=-0.4$, $\tau=0.4$, and (d) $K=-0.6$, $\tau=0.75$. Control is switched on at $t=3000$.

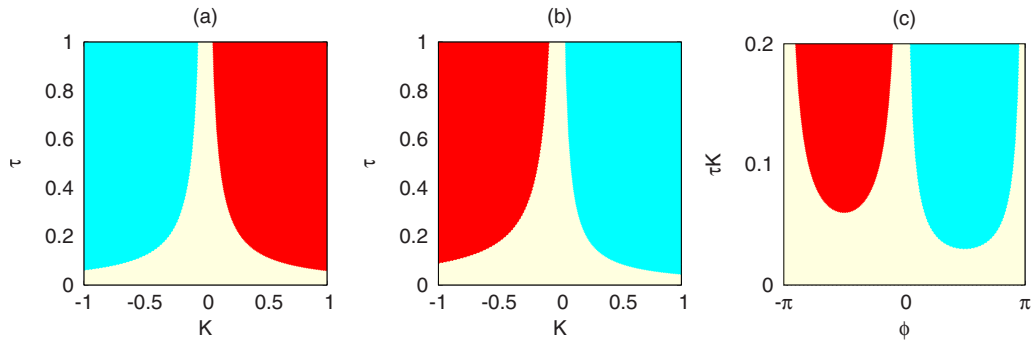


FIG. 6. (Color online) Phase diagram for control of traveling waves. (a) Activator control. (b) Inhibitor control. (c) Phase diagram for nondiagonal control (15) of traveling waves. (a) Specific final states are: the middle region is a stable traveling wave (beige), to the left of it is a stationary Turing pattern (cyan), and to the right is a bistability between traveling waves and a trivial steady state E_0 (red). In (b) and (c) the order of regimes from left to right is reversed. Parameter values are $a=0.022$, $b=0.053$, $D_u=2 \times 10^{-5}$, and $D_v=10^{-5}$.

IV. CONTROL OF TRAVELLING WAVES

In this section we consider a situation when without control the system supports stable traveling waves. By virtue of choosing periodic boundary conditions, if there is more than one pulse in the interval, all pulses are elastically reflected from each other and move without changes through the boundaries.

As before, we start our analysis by considering single-species control of the form (11), and the results are shown in Figs. 6(a) and 6(b). In the case of activator control with $K < 0$ or inhibitor control with $K > 0$, the stable traveling waves are eventually transformed into stable spatially periodic Turing patterns by means of wave splitting, as shown in Fig. 7(a). As has been noted by Petrov *et al.*,³⁰ this happens due to the fact that the medium becomes saturated with waves which are reflected from each other. Numerical simulations suggest that the higher the value of $|K|\tau$, the longer it will take for the wave splitting to result in a stationary spatially periodic pattern and that TDFC can stabilize unstable multispikes steady states. This provides a mechanism of transformation from a stable propagating pulse to a stable Turing pattern. Finally, we note that the activator ($K > 0$) or inhibitor ($K < 0$) control shown in Figs. 6(a) and 6(b) can only provide the bistability between a homogeneous trivial state E_0 and traveling waves. For illustration purposes, we show in

Fig. 7(b) the transition to stable traveling pulses, however, in the same parameter regime the system may also evolve into a homogeneous state E_0 .

Figure 6(c) shows the effects of mixed control on the dynamics of traveling waves with some similarity to the earlier picture of mixed control of spatiotemporal chaos [Fig. 3(c)]. There is still almost no dependence on the strength and sign of activator control, but the region of stationary Turing patterns is noticeably larger than that of bistability between a homogeneous trivial steady state E_0 and a traveling wave. As in the case of spatiotemporal chaos, the diagonal control of traveling waves does not qualitatively change the dynamics, and the system remains in the state of supporting elastic traveling waves.

When compared to recent work on TDFC of traveling pulses in the FitzHugh–Nagumo model,¹⁷ our results show both some similarities and also certain differences. In both cases, the control domain of the inhibitor control is smaller than that of the activator control. It is worth noting that in Ref. 17 nondiagonal control was not applied in the form of mixed control (15), involving both activator and inhibitor variables, but was in the form of

$$A = \begin{pmatrix} 0 & \pm 1 \\ 0 & 0 \end{pmatrix} \quad (uv - \text{control})$$

or

$$A = \begin{pmatrix} 0 & 0 \\ \pm 1 & 0 \end{pmatrix} \quad (vu - \text{control}).$$

Suppression of the traveling pulse in case of uv -control was only possible for the minus sign, while in case of vu -control suppression was only found for the plus sign, following a strict symmetry with respect to the operation $K \rightarrow -K$. In some sense this is similar to Fig. 8 where the uniform steady state (red) can be stabilized only for negative uv feedback or positive vu feedback.

The main difference, however, is that the nondiagonal control of traveling pulses in the Gray–Scott model in the form Eq. (15) is successful for both signs of the control strength K , even though for one sign of K it produces stationary Turing patterns and for another it leads to a homoge-

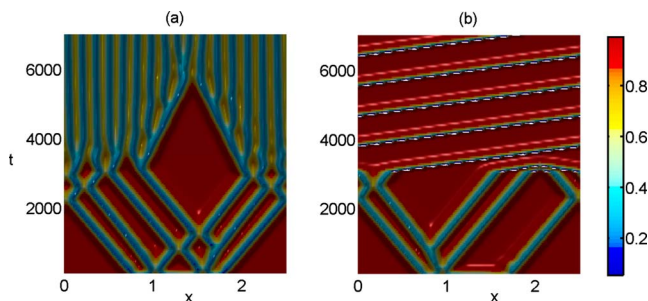


FIG. 7. (Color online) Space-time plot of control of traveling waves. (a) Activator control: Development of a stationary Turing pattern. (b) Inhibitor control: Transition to traveling wave. Parameter values are $a=0.022$, $b=0.053$, $D_u=2 \times 10^{-5}$, $D_v=10^{-5}$, (a) $K=-0.5$, $\tau=0.6$ and (b) $K=-0.8$, $\tau=0.4$. Control is switched on at $t=3000$.

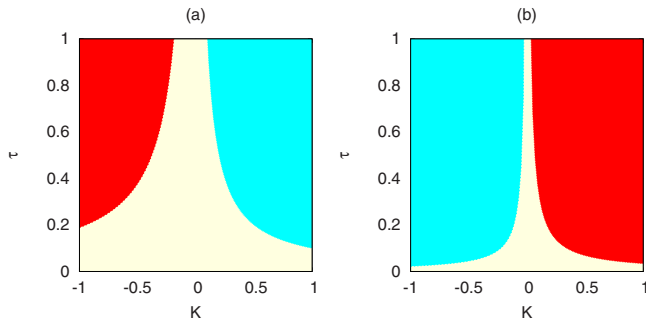


FIG. 8. (Color online) Phase diagram for control of travelling waves. (a) Activator uv -control. (b) Inhibitor vu -control. (a) Specific final states are: the middle region is a stable traveling wave (beige), to the left of it is a bistability between traveling waves and a trivial steady state E_0 (red), and to the right is a stationary Turing pattern (cyan). In (b) the order of regimes from left to right is reversed. Parameter values are $a=0.022$, $b=0.053$, $D_u=2 \times 10^{-5}$, and $D_v=10^{-5}$.

neous trivial steady state E_0 . Finally, we note that vu -control is able to stabilize the uniform steady state or stationary Turing patterns for significantly smaller values of K and τ as compared to uv -control. Also, Fig. 8 shows that the roles of activator and inhibitor are reversed for the same values of K and τ when compared to Fig. 6.

V. CONCLUSIONS

In this paper we have studied the effects of TDFC on the dynamics of the Gray–Scott model. When the original system is in the spatiotemporally chaotic state, an activator control with $K < 0$ or inhibitor control with $K > 0$ transforms it into a homogeneous nontrivial steady state E_1 . A much wider range of possible states can be reached for an activator control with $K > 0$ or inhibitor control with $K < 0$, and these include the stable mixed Turing–Hopf modes, coarsening, as well as a regime of bistability between a stable pulse and a homogeneous trivial state E_0 . Diagonal control appears to be ineffective as it cannot control the spatiotemporal chaos. For mixed type of TDFC, the simulations suggest that the sign of nondiagonal terms in the coupling matrix plays a crucial role in determining the final state of the system. As in the case of global TDFC, the local control is unable to stabilize uniform periodic oscillations.

When the TDFC is applied to traveling pulses of the Gray–Scott model, there are two possibilities for the final state. Activator control with $K < 0$ or inhibitor control with $K > 0$ transforms the system into a regime of wave splitting, and after the medium is saturated with the waves, it settles on a stationary spatially periodic Turing pattern. The higher is the value of $|K|\tau$, the longer it takes for the system to reach such a pattern. On the other hand, activator control with $K > 0$ or inhibitor control with $K < 0$ suppresses spatial inhomogeneities and provides bistability between a stable traveling pulse and a homogeneous trivial state, similar to the control of spatiotemporal chaos.

The control schemes studied in this paper can be used for control of spatiotemporal chaos in other spatially extended systems. While stabilization of uniform periodic oscillations may remain elusive, local TDFC can provide a variety of interesting dynamical regimes, from stationary patterns to mixed modes and traveling localized pulses. Numerical simulations suggest that in many cases the control strength does not have to be very high, provided time delay is large enough. This interplay between the control strength and time delay should prove beneficial for the development of experimental implementation of specific control schemes.

ACKNOWLEDGMENTS

Y.K. acknowledges the support from the EPSRC via EPSRC Postdoctoral Fellowship (Grant No. EP/E045073/1). This work was partially supported by Deutsche Forschungsgemeinschaft in the framework of Sfb 555.

- ¹*Handbook of Chaos Control*, edited by E. Schöll and H. G. Schuster (Wiley-VCH, Weinheim, 2008).
- ²E. Ott, C. Grebogi, and J. A. Yorke, *Phys. Rev. Lett.* **64**, 1196 (1990).
- ³K. Pyragas, *Phys. Lett. A* **170**, 421 (1992).
- ⁴T. Dahms, P. Hövel, and E. Schöll, *Phys. Rev. E* **76**, 056201 (2007).
- ⁵P. Hövel and E. Schöll, *Phys. Rev. E* **72**, 046203 (2005).
- ⁶S. Schikora, P. Hövel, H.-J. Wünsche, E. Schöll, and F. Henneberger, *Phys. Rev. Lett.* **97**, 213902 (2006).
- ⁷B. Fiedler, V. Flunkert, M. Georgi, P. Hövel, and E. Schöll, *Phys. Rev. Lett.* **98**, 114101 (2007).
- ⁸Y. Kuramoto, *Chemical Oscillations, Waves and Turbulence* (Springer-Verlag, Berlin, 1984).
- ⁹C. Beta and A. S. Mikhailov, *Physica D* **199**, 173 (2004).
- ¹⁰M. Kim, M. Bertram, M. Pollmann, A. von Oertzen, A. S. Mikhailov, H. H. Rotermund, and G. Ertl, *Science* **292**, 1357 (2001).
- ¹¹K. A. Montgomery and M. Silber, *Nonlinearity* **17**, 2225 (2004).
- ¹²C. M. Postlethwaite and M. Silber, *Physica D* **236**, 65 (2007).
- ¹³O. Beck, A. Amann, E. Schöll, J. E. S. Socolar, and W. Just, *Phys. Rev. E* **66**, 016213 (2002).
- ¹⁴G. Franceschini, S. Bose, and E. Schöll, *Phys. Rev. E* **60**, 5426 (1999).
- ¹⁵J. Unkelbach, A. Amann, W. Just, and E. Schöll, *Phys. Rev. E* **68**, 026204 (2003).
- ¹⁶J. Schlesner, V. Zykov, H. Engel, and E. Schöll, *Phys. Rev. E* **74**, 046215 (2006).
- ¹⁷M. A. Dahlem, F. M. Schneider, and E. Schöll, *Chaos* **18**, 026110 (2008).
- ¹⁸A. Ahlborn and U. Parlitz, *Phys. Rev. E* **75**, 065202(R) (2007).
- ¹⁹M. E. Bleich and J. E. S. Socolar, *Phys. Rev. E* **54**, R17 (1996).
- ²⁰M. Münkel, F. Kaiser, and O. Hess, *Phys. Rev. E* **54**, 3868 (1997).
- ²¹P. Gray and S. K. Scott, *Chem. Eng. Sci.* **39**, 1087 (1984).
- ²²K. J. Lee, W. D. McCormick, Q. Ouyang, and H. L. Swinney, *Science* **261**, 192 (1993).
- ²³W. Mazin, K. E. Rasmussen, E. Mosekilde, P. Borckmans, and G. Dewel, *Math. Comput. Simul.* **40**, 371 (1996).
- ²⁴Y. Nishiura and D. Ueyama, *Physica D* **150**, 137 (2001).
- ²⁵A. S. Mikhailov and K. Showalter, *Phys. Rep.* **425**, 79 (2006).
- ²⁶A. De Wit, D. Lima, G. Dewel, and P. Borckmans, *Phys. Rev. E* **54**, 261 (1996).
- ²⁷W. Just, M. Bose, S. Bose, H. Engel, and E. Schöll, *Phys. Rev. E* **64**, 026219 (2001).
- ²⁸M. Meixner, A. De Wit, S. Bose, and E. Schöll, *Phys. Rev. E* **55**, 6690 (1997).
- ²⁹A. P. A. Fischer, O. K. Andersen, M. Yousefi, S. Stolte, and D. Lenstra, *IEEE J. Quantum Electron.* **36**, 375 (2000).
- ³⁰V. Petrov, S. K. Scott, and K. Showalter, *Philos. Trans. R. Soc. London, Ser. A* **347**, 631 (1994).